

# A Power Saving Scheme for IEEE 802.15.3d THz Wireless Communication Links

Wafa Hedhly, Osama Amin, Basem Shihada and Mohamed-Slim Alouini

**Abstract**—Terahertz (THz) band spans the frequencies lying between 0.1 and 10 THz and represents the gap between millimeter waves and Infrared bands. THz will play an influential role in mitigating the spectrum resources shortage to meet the exponential growth of services and wireless devices. Standardization activities are being carried out to regulate the THz band's exploitation under the IEEE 802.15 standardization project. Despite the generous bandwidth, THz communications suffer from high pathloss and attenuation due to Molecular Absorption. As such, THz systems need to use extra power, suitable antennas, and enhanced signal processing and communication techniques to compensate for different signal attenuation sources. In this paper, we propose a new operation mode for the IEEE standard 802.15 to save the power transmission requirement while achieving the required data rate. Hence, less battery or antenna size is needed to support the same communication link quality. To this end, we optimize the power, modulation scheme, and channel allocation to minimize the total transmitted power keeping a minimum quality-of-service. Moreover, the design captures the effect of **humidity on the system performance**.

**Index Terms**—Terahertz communication, IEEE 802.15.3d standard, pathloss model, interference channel, molecular absorption, resource allocation, power saving.

## 1 INTRODUCTION

**N**OWADAYS, 5G technology is being deployed with several new features to end-users, **including high data rates up to 20 Gbps downlink peak rate and 4 ms user plane latency in Enhanced Mobile Broadband (EMBB)** [1]. However, the urge for extra connection speed and improved communication link performance, in general, are persisting, which motivates researchers to pursue various horizons. In this context, the THz band is one of the promising enabling technologies for next-generation wireless communication networks [2]. Data rates anticipated by 6G wireless communication systems shall hit the 1 Tbps data rate limit. The THz band can intervene and ensure such tremendous data rates requirement with proper signal processing and communication techniques and appropriate implemented hardware performance. The THz band is an unexploited frequency spectrum lying between 100 GHz and 10 THz, in the gap between microwave and infrared bands, c.f. Fig. 1, where both being extensively studied and used. **Researchers hope to relax the heavy use of the microwave band and offer more data-consuming applications using the large available bandwidth in the THz spectrum, conveying outstanding communication rates without relying on high order modulation or diversity techniques** [3]. THz frequencies are a promising candidate for several applications such as nanonetworks and on-chip communication [4], fixed radio links and personal area networks [5], backhaul communication [6] and several molecules detection [7].

**THz radiation undergoes different physical and chemical interactions with the propagation environment than**

**lower frequency bands.** Due to its small wavelength compared to the dimensions of surface imperfections, THz waves undergo a different reflection process than the typical sub-6 GHz communication, which was heavily studied to characterize the phenomena of reflection, scattering, and diffraction, and their impact on the signal's quality [8]–[10]. Another aspect is the scattering of the EM wave due to the small wavelength of the wave compared to the dimensions of surface imperfections. The level of surface roughness controls the EM wave scattering direction and amount. **In addition to the traditional spreading loss, THz waves, characterized by a tiny wavelength, go through the molecular absorption leading to severe frequency selectivity** [11]. The molecular absorption is caused by the resonance of some molecules existing in the medium. This peculiarity is to be taken into consideration in channel modeling and systems design. THz channel modeling has been an important research direction for investigating THz capabilities and mainly trying to cope with the channel imperfections [7], [11]–[13].

Recently, several research studies designed THz communication systems and optimized their performance to meet the expected next-generation communication applications. Achievable rate investigation was one of the most visited topics in the literature since it is one of the most crucial gains of using THz signals. To mitigate the impacts of high distance-based attenuation and frequency selectivity, signal processing and communication techniques are adopted to enable proper operations of THz systems. Designing adaptive systems is one of the robust solutions that mitigate different types of challenges. The use of high gains for the transmit and receive antennas is imperative to have one directed beam capable of beating the severe channel fading. Several parameters in THz systems can be **tuned**, such as modulation scheme and transmitted power [14]–

W. Hedhly, O. Amin, B. Shihada and M.-S. Alouini are with CEMSE Division, King Abdullah University of Science and Technology (KAUST), Thuwal, Makkah Province, Saudi Arabia. E-mail: {wafa.hedhly, osama.amin, basem.shihada, slim.alouini}@kaust.edu.sa.

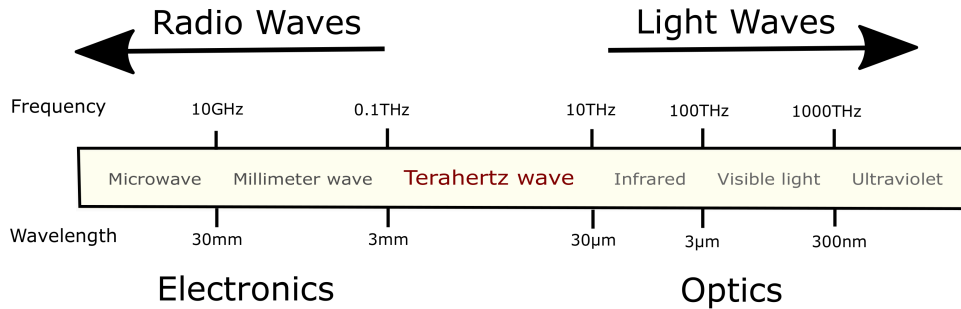


Figure 1: Terahertz spectrum.

[22]. In [14], the authors proposed an adaptive resource allocation scheme to maximize the communication range by adjusting the power, modulation, and spectral windows. A similar work has been done in [15] with an additional analysis of the interference between different bands. In [22], the achievable rate in an indoor setup was investigated where multiusers communicate with several access points operating at THz band, achieving 20 Gbps for every user. **Intelligent Reflecting Surfaces (IRS) were utilized in [18] to maximize the sum-rate of user equipment by tuning the individual transmit powers and IRS-related parameters over the THz band.** The study in [19] tried to enhance data rates in Multiple-Input Multiple-Output (MIMO) THz systems. Furthermore, several research works have been done to adopt THz communications in different scenarios, such as designing a joint time scheduling and power allocation for mesh networks [21], and optimizing energy efficiency for Non-Orthogonal Multiple Access (NOMA) MIMO systems [20]. The objective of the previously mentioned research studies was to maximize the transmission distance or the achievable rate. However, it is essential to monitor the THz power requirements needed to mitigate the corresponding path loss by optimizing different system resources.

Adopting a high antenna gain or a generous power budget can improve the THz link performance and mitigate different types of THz channel attenuation. Moreover, the high-gain antenna can eliminate the Non-Line-of-Sight (NLoS) components and form a narrow beam pointing towards the desired direction. It focuses the radiation in a specific direction, unlike omnidirectional antennas that distribute the radiation in all directions. However, such promising assumptions are not always affordable due to device size constraints and infeasible power requirements. Installing a very high antenna gain, i.e., exceeding 50 dB, may not always be appropriate due to its large size that does not suit the average device size. Aperture antennas such as parabolic antennas are characterized by a large aperture and capture more energy from the coming signal [23]. Achieving higher gain requires increasing the size when designing the antenna [24]. For example, a parabolic antenna with a diameter of 6 cm can achieve a directivity gain of 40 dB [25]. To improve the antenna gain, we should use a large antenna size with a diameter of 20 cm [26]. Moreover, portable devices have constraints on the maximum battery power that is also

governed by the device's size. For these reasons, designing power saving scheme is crucial, especially for small devices with limited energy capabilities and size constraints. To the best of our knowledge, there is no effort paid in saving the power requirement of THz links to meet practical limitations.

In this paper, we propose a power-saving scheme for the first regularized THz standard IEEE 802.15.3d to allow using compact devices with less bulky power supplies and antennas. In this regard, we provide a detailed study of the THz pathloss model by capturing several peculiarities, including the THz band's physical characteristics such as **atmospheric** conditions, distance, and frequency, using the data provided in the **High-resolution TRANsmission molecular absorption database (HITRAN)** database [27]. Then, we develop a strategic resource allocation scheme for IEEE 802.15 standard to save the transmitted power requirement by tuning the allocated power, channels, and modulation scheme while keeping a minimum rate requirement. Although the resource allocation scheme deals with a mixed integer nonlinear programming, we propose a simple, intelligent resource allocation scheme that achieves notable power-saving performance for the IEEE THz standard 802.15.3d.

The rest of the paper is organized as follows. In section II, we detail the channel attenuation factors in the THz spectrum. Then, we describe in Section III the system model that uses the IEEE 802.15 standard. In section IV, we solve the resource allocation problem and propose the power saving scheme. Finally, we present some numerical results in Section V followed by a conclusion in Section VI.

## 2 PATHLOSS MODEL IN THE THZ BAND

In this section, we explain, step by step, the pathloss model in the THz band, considering the peculiarities of the THz wave and their impact on how it is attenuated in free space. One of the main characteristics of the THz channel is its high pathloss due to two major facts:

- 1) **Spreading loss:** Due to the high frequency of THz waves, the latter undergo very high spreading loss compared to other bands. For a wave propagating at a frequency  $f$  and traveling a distance  $d$ , the attenuation caused by free-space pathloss is expressed as follows,

$$A_{\text{spr}} = 20 \log_{10} \left( \frac{4\pi f d}{c} \right), \quad (1)$$

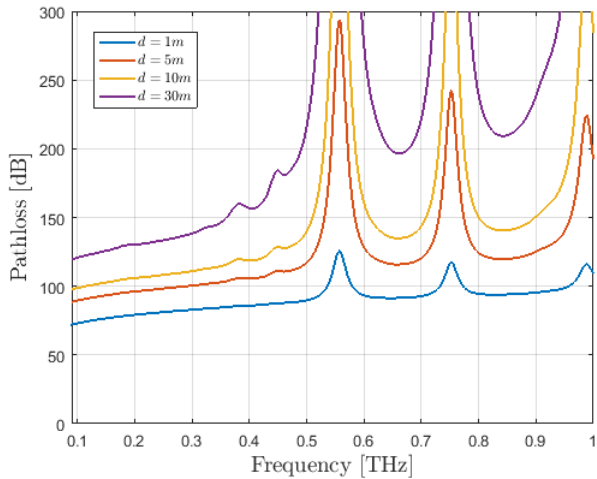


Figure 2: Pathloss in the THz band for different transmit distances

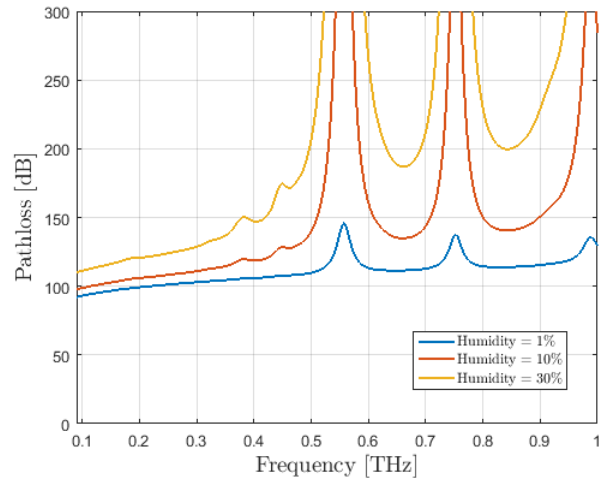


Figure 3: Pathloss in the THz band for different humidity levels

where  $c = 3 \times 10^8$  m/s is the velocity of the wave.

- 2) **Molecular absorption:** Terahertz channel suffers from a high attenuation due to molecular absorption. In fact, when an EM wave is propagating through a medium, the molecules are excited at specific frequencies, and the atoms start to vibrate (rotation, translation and torsion). Therefore, part of the energy is consumed in these motions, after being converted to kinetic energy [28]. The wave is then attenuated. It's worth mentioning that water vapor has the main contribution to the molecular absorption, creating several peaks of attenuation in the Terahertz band [28]. The attenuation caused by the molecular absorption to an electromagnetic wave propagating at frequency  $f$  is expressed as follows,

$$A_{\text{abs}} = \exp(k(f) d), \quad (2)$$

where  $d$  is the traveled distance and  $k$  is the medium absorption coefficient which depends on the molecular composition of the considered medium **including the gases and the number of molecules per unit volume and other environmental parameters like the pressure and the temperature.** [28]. In this context, the HITRAN Database [29] is widely used as a standard to compute atmospheric transmission of EM waves (spectroscopy and radiative transfer through gases). **The overall molecular absorption is the aggregate effect of all existing gases in the medium. Water molecules have the most significant contribution to the molecular absorption. The detailed analysis of the molecular absorption is provided in Appendix A.**

The overall pathloss in the THz band can be seen in Fig.2 versus the frequency and for different transmit ranges. From Fig.2, we can see clearly that pathloss is a main limitation to THz communication systems when it comes to transmit ranges. At long distances, pathloss peaks become more pronounced and the set of usable bands gets smaller.

**Furthermore,** humidity is a key parameter in the THz band since the pathloss increases exponentially with the

number of water molecules in the medium. For this reason, we plot in Fig.3, the pathloss versus the frequency for different values of humidity and for a fixed distance of 10 meters. We can observe similar behavior as the effect of distance, more significant peaks with very high pathloss for high humidity. This phenomenon can be considered as a limitation to THz systems in regions or seasons with high humidity levels. We provide a Matlab code that computes pathloss in the THz band applying the previously explained steps <sup>1</sup>.

### 3 SYSTEM DESCRIPTION

In this section, we discuss the architecture of our THz system based on the recently approved THz IEEE 802.15.3d standard. We then define the interference model and the successfully delivered data rate as a performance metric measurement.

#### 3.1 IEEE 802.15.3 Standard

Establishing THz communication systems is being initiated through different research work and standardization activities [32]. In 2017, the first THz standard for the frequency range between 252 GHz and 325 GHz was defined, where physical layer modes were proposed to enable data rates of up to 100 Gbps using eight different bandwidths between 2.16 GHz and 69.12 GHz [31] as depicted in Fig.4. The objective of the proposed modes is either to achieve tremendous data rates or simple system design using appropriate coding techniques, modulation schemes and bandwidth allocations. Requirements in terms of Bit Error Rates (BER) were determined to be in the order of  $10^{-12}$ , using specific Forward Error Correction (FEC) rates [31]. The adopted channel coding are Reed-Solomon (RS) code and Density Parity Check (LDPC) codes [30].

1. Link to the code with the necessary files to run it: <https://github.com/wafa4/PathlossTHz>

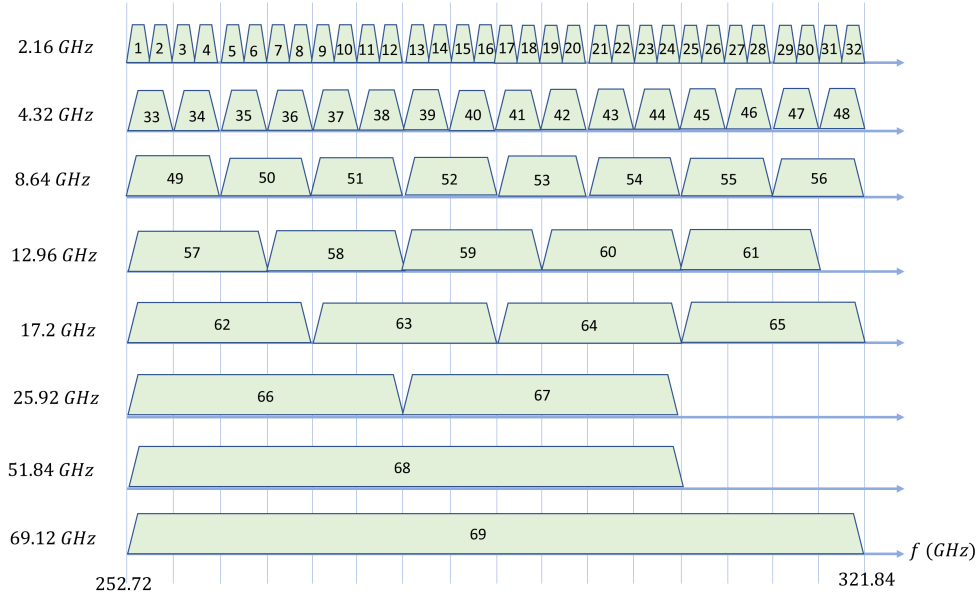


Figure 4: Channel plan of the THz standard IEEE 802.15.3d [30], [31].

The IEEE 802.15.3d standard is mainly deployed for point-to-point links and does not consider multiple access scenarios and interference mitigation to relax the requirements on the access control. It only supports the connection between two devices, also called a pairnet [33]. In particular, backhaul and fronthaul applications are considered suitable for the THz frequency range of the standard [34].

### 3.2 Channel Characterization

Before delving to the system model, we present in the following, the transmission channels used to transmit the signal in the THz band. It's important to mention that with high antenna gains, the antenna's narrow beam will be focused in the LoS direction, and we can ignore the reflected and scattered rays.

Since the THz channel is firmly frequency selective, the channel response is not flat, and the transmitted signal will be highly distorted. As such, the IEEE 802.15.3d THz standard is regularized to divide the band into several sub-channels with a frequency-flat performance. The entire adopted band extends from 252.72 GHz to 321.84 GHz, and is divided into several sub-channels with a frequency flat gain [35]. The width of each transmission subchannel is 2.16 GHz, which results in  $L = 32$  subchannels [31], as depicted in Fig. 4.

As mentioned in [35], the coherence bandwidth can be expressed as

$$B_c = \frac{1}{\tau_{\text{rms}}} = \frac{1}{t_{\text{MP}} - t_{\text{LoS}}}, \quad (3)$$

where  $\tau_{\text{rms}}$  is the delay spread,  $t_{\text{MP}}$  and  $t_{\text{LoS}}$  are the arrival times of the latest multipath component and the LoS component to the receiver, respectively. Since we consider only the LoS component in our model,  $t_{\text{MP}}$  can be considered very close to  $t_{\text{LoS}}$  and therefore, the coherence bandwidth

increases considerably. Furthermore, when high directive antennas are used, the coherence bandwidth can reach 60 GHz [36]. Therefore, the channel response over each sub-band is expressed as follows,

$$h(t) = \alpha_{\text{LoS}} \delta(t - t_{\text{LoS}}) \quad (4)$$

where  $\alpha_{\text{LoS}}$  and  $t_{\text{LoS}}$  are the gain and the delay, respectively, between the transmitter and receiver of the LoS path.

The THz channel is characterized by a significant additional source of attenuation, which is the molecular absorption. **Therefore, the noise in the THz channel is not white since it mainly comes from the molecular absorption, but it can be approximated by a white Gaussian noise with power  $P_N = 10 \log_{10}(K_B T B) = -80$  dBm for  $B = 2.16$  GHz,  $T = 298$  K [14].**

### 3.3 System model

Consider a point-to-point communication system, where a transmitter is communicating with a receiver over the THz band lying between 252.72 GHz and 321.84 GHz. The transmitter accesses the spectrum with a maximum power budget of  $p_{\text{max}}$ , where the power can be divided between the 32 available subchannels or windows<sup>2</sup>. For a window  $w$ , where  $w \in \{1, \dots, L\}$  and  $L$  being the number of accessed windows, the transmitter sends a part  $p_w$  of the total power budget, i.e.,  $p_{\text{max}}$ . We denote by  $h_w$  the channel response over each window  $w$ , as described in (4). The overall system is subject to **Additive White Gaussian Noise (AWGN)** with zero mean and variance  $\sigma^2$ . Channel-to-noise ratios (CNR) are defined as  $\Gamma_w = |h_w(d)|^2 / \sigma^2$ , where  $d$  is the distance between transmitting and receiving nodes. We denote the interference-to-noise over a window  $w$  by  $\mathcal{I}_w$ , which will be

<sup>2</sup> In the rest of the paper, we use the terms subchannels and windows, equivalently and interchangeably.

detailed in the next section. The gain of the transmit and receive antennas are respectively,  $G_t$  and  $G_r$ .

The transmitted message uses adaptive **Quadrature Amplitude Modulation (QAM)** to maximize the data rate and increase the bandwidth efficiency. Over each window  $w$ , we transmit  $k_w$  bits with a modulation order of  $M_w = 2^{k_w}$ . The source and the receiver can be equipped with high directive antennas to avoid scattered rays and focus most of the energy in the direct path, which helps to beat the high channel pathloss.

### 3.4 Interband interference

Despite the use of high directive transmit and receive antennas, leakage can occur from subwindows and cause non-negligible interference to adjacent bands and that needs to be taken into consideration throughout the analysis. An approximation of the InterBand Interference (IBI) is expressed according to [14] as follows:

$$IBI_w \sim \mathcal{N} \left( 0, \int_{f_w} \sum_{v, v \neq w}^L p_v |H_v(f_w)|^2 \sum_{m=1}^{N_M} \alpha_v(m) |df_w| \right) \quad (5)$$

where  $N_M$  is the number of multipath components,  $P_v$  is the transmitted power at the  $v$ -th window and  $H_v$  is the adopted pulse shape over this window. The scenario when  $N_M = 1$  denotes to the LoS, which can occur by using high directive antennas and  $H_v$  can be a raised cosine pulse shaping, which is assumed to be used across different subchannel, i.e.,  $H_v = H(f)$ ,  $\forall v \in \{1, \dots, L\}$ . Thus, the IBI will reduce to,

$$IBI_w \sim \mathcal{N} \left( 0, \int_{f_w} \sum_{v, v \neq w}^L p_v |H_v(f_w)|^2 \alpha_{v, \text{LoS}} |df_w| \right). \quad (6)$$

Since, we divided the entire bandwidth to several subchannels to have frequency flat transmission windows,  $\alpha_{v, \text{LoS}}$  is constant. Therefore, the Signal-to-Noise Ratio (SNR) of the interference signal is expressed as follows

$$\mathcal{I}_w = \sum_{v, v \neq w}^L \frac{p_v}{\sigma^2} |\alpha_{v, \text{LoS}}|^2 S_{\text{leak}, w} \quad (7)$$

where  $S_{\text{leak}, w}$  is the leakage from  $v$ -th subchannel on the  $w$ -th one, which depends on the waveform adopted in the  $v$ -th subchannel, where  $S_{\text{leak}, w}$  is found from

$$S_{\text{leak}, w} = \int_{f_w} |H_v(f_w)|^2 df_w. \quad (8)$$

In case we use a Raised Cosine filter, for the pulse shaping, with roll-off factor  $\beta_F$  and a symbol time  $T_s$ , its frequency response is written as [37]

$$H(f) = \begin{cases} T_s, & |f| \leq \frac{1-\beta_F}{2T_s} \\ 0, & |f| \geq \frac{1+\beta_F}{2T_s} \\ \frac{T_s}{2} \left( 1 + \cos \left( \frac{\pi T_s}{\beta_F} \left( |f| - \frac{1-\beta_F}{2T_s} \right) \right) \right), & \text{otherwise.} \end{cases} \quad (9)$$

Therefore, the SINR on the  $w^{\text{th}}$  subwindow is written now as follows,

$$\gamma_w = \frac{G_t G_r \Gamma_w P_w}{G_t G_r \mathcal{I}_w + 1} \quad (10)$$

### 3.5 Rate Expression

In the following discussion, we evaluate the successfully delivered data rate from using several subchannels. First, we assume the transmit power vector of different windows is  $p = [p_1, \dots, p_L]$ . Also, we let the  $w$ -th subchannel of bandwidth  $B$  transmit  $k_w$  bit/second/symbol, allowing to express the successfully delivered data rate as follows,

$$R_L = \sum_{w=1}^L B k_w (1 - \eta_w(p)), \quad (11)$$

where  $\eta_w$  is the error probability over window  $w$  and is expressed in terms of  $\gamma_w$  as [38],

$$\eta_w(p) = 4 \left( 1 - \frac{1}{\sqrt{M_w}} \right) \mathcal{Q} \left( \sqrt{\frac{3}{M_w - 1} \gamma_w(p)} \right) - 4 \left( 1 - \frac{1}{\sqrt{M_w}} \right)^2 \mathcal{Q} \left( \sqrt{\frac{3}{M_w - 1} \gamma_w(p)} \right)^2, \quad (12)$$

where,  $\gamma_w$  is the SINR over window  $w$ , expressed as following

$$\gamma_w(p) = \frac{G_t G_r \Gamma_w P_{\text{shaping}} p_w}{G_t G_r \mathcal{I}_w(p) + 1} \quad (13)$$

where  $P_{\text{shaping}}$  is the pulse shaping term computed from (9) as,

$$P_{\text{shaping}} = \int_{f_w} |H_w(f_w)|^2 df_w.$$

Interference terms in (13) are computed from (7).

## 4 POWER SAVING BASED RESOURCE ALLOCATION SCHEME

In this section, we formulate the corresponding optimization problem to allocate the available resources to minimize the system's power consumption. Then, we analyze the problem and propose a suitable solution.

### 4.1 Problem Formulation

The objective of this work is to strategically allocate the transmission subchannels, corresponding power, and modulation scheme while allowing the successful delivery of a minimum data rate. We formulate the relevant optimization problem as follows,

$$\begin{aligned} \min_{p_w, k_w} \quad & \sum_{w=1}^L p_w \\ \text{subject to} \quad & \text{C1: } R_L \geq R_{\min} \\ & \text{C2: } \sum_{w=1}^L p_w \leq p_{\max} \\ & \text{C3: } 0 \leq k_w \leq k_{\max}, k_w \in \mathcal{K}, \forall w \in \{1, \dots, L\} \\ & \text{C4: } p_w \geq 0, \quad \forall w \in \{1, \dots, L\}, \end{aligned} \quad (14)$$

where  $\mathcal{K}$  is the set of square M-QAM with maximum  $k_{\max}$  bits per symbol and  $R_{\min}$  is the minimum data rate required to be achieved of the THz link.

**The objective of this problem is to minimize the aggregate power consumption  $\sum_{w=1}^L p_w$  over the  $L$  utilized transmission windows by tuning the individual**

transmit powers  $p_w$  and the number of allocated bits  $k_w$ . The problem formulation ensures certain conditions on the decision parameters through several constraints. To maintain a minimum QoS, the achievable rate of the system is ensured to not fall below a minimum threshold  $R_{\min}$  through (C1). The second constraint (C2) verifies that the total power does not exceed the maximum budget  $p_{\max}$ . The third constraint (c3) governs the allocation of bits per window  $k_w$  to keep it within the considered range  $\mathcal{K}$ . Last, the transmit power  $p_w$  is always kept greater than zero through (C4).

The optimization (14) lies under the category of nonlinear mixed-integer problems that are not easy to be analyzed and solved, especially that the complexity grows exponentially with the cardinality of  $\mathcal{K}$ . In the following section, we propose a simplified optimization scheme that can improve power-saving by addressing (14) in a recursive fashion.

## 4.2 Recursive Optimization Scheme

In this section, we propose an efficient and computationally inexpensive scheme for (14). To this end, we first introduce new parameters:  $p_T$  that is the total power used for data transmission across all subchannels, and  $\alpha_w \in [0, 1]$  that are the distribution factors among different subchannels, i.e.,  $p_w = \alpha_w p_T$ ,  $w$  denoting a subchannel. Therefore, the problem (14) is written equivalently as,

$$\begin{aligned} \min_{p_T, \alpha_w, k_w} \quad & p_T \\ \text{subject to} \quad & R_L(p_T, \alpha_w) \geq R_{\min} \\ & \sum_{w=1}^L \alpha_w = 1 \\ & 0 \leq p_T \leq p_{\max} \\ & 0 \leq k_w \leq k_{\max}, \quad k_w \in \mathcal{K}, \forall w \in \{1, \dots, L\} \\ & \alpha_w \geq 0 \quad \forall w \in \{1, \dots, L\}, \end{aligned} \quad (15)$$

where we assume the subchannels are sorted according their channel gain in a descending order; without loss of generality.

To solve (15), we propose a recursive approach by assuming the availability of  $(n-1)$  subchannels' solution in terms of the transmitted power,  $p_{T,n-1}$ , the power distribution ratio,  $(\alpha_1, \alpha_2, \dots, \alpha_{n-1})$ , and the transmitted number of bits,  $(k_1, k_2, \dots, k_{n-1})$ . Then, we use these solutions to allocate the resources for the  $n$  subchannels scenario in a way that results in performance improvement. As such, we use the same power distribution ratio of the  $(n-1)$  subchannels, and the same modulation scheme. Then, we optimize the power distribution between the  $n^{\text{th}}$  subchannel and the  $n-1$  subchannels along with the candidate modulation scheme and the total power in a way that minimize the total power consumption and keep the minimum rate requirements.

To do so, we define  $\beta \in [0, 1]$  as a distribution factor such that  $p_n = (1-\beta)p_{T,n}$  and  $\sum_{w=1}^{n-1} p_w = \beta p_{T,n}$ , where  $p_{T,n}$  is the total transmission power when we use  $n$  subchannels with  $p_w = \beta \alpha_w p_{T,n}$ ,  $1 \leq w \leq n-1$ ,  $\sum_{w=1}^{n-1} \alpha_w = 1$  and  $\beta \sum_{w=1}^{n-1} \alpha_w + (1-\beta) = 1$ . The last expression implies that  $(1-\beta)p_{T,n}$  is allocated to the  $n^{\text{th}}$  window and the

remaining power, i.e.  $\beta p_{T,n}$  is distributed between the  $n-1$  windows using the factors  $\alpha_w$ ,  $1 \leq w \leq n-1$  previously calculated. Therefore, instead of computing the optimal power allocations per each window, the problem is simplified to computing the optimal values of  $\beta$  and  $p_{T,n}$ .

Hence, we express the recursive optimization problem as follows

$$\begin{aligned} \min_{p_{T,n}, \beta, k_n} \quad & p_{T,n} \\ \text{subject to} \quad & R_n(p_{T,n}, \beta) \geq R_{\min} \\ & 0 \leq \beta \leq 1 \\ & 0 \leq p_{T,n} \leq p_{\max} \\ & 0 \leq k_n \leq k_{\max}. \end{aligned} \quad (16)$$

We solve (16) by fixing  $k_n$  and  $p_{T,n}$ , where arbitrary values can be chosen for  $k_n$  to look for the best solution among possible values of  $k_n$ , and  $p_{T,n}$  takes initially the value of  $p_{T,n-1}$ . Then, we find  $\beta$  by studying the behavior of  $R_n(p_{T,n}, \beta)$  versus  $\beta$  as shown in Appendix B, where we show that  $R(\beta)$  has at least one peak in the interval  $[0, 1]$ . Since we considered ordered subchannels, the  $n^{\text{th}}$  subchannel will have the lowest channel gain. Thus, it is expected to have least power especially since it has the least contribution to the achievable rate due to its lowest channel gain. For this reason,  $\beta$  should be close to 1 to minimize the power portion of the  $n^{\text{th}}$  channel. Then, the best solution is the **closest**  $R_n(p_{T,n}, \beta)$  peak to  $\beta = 1$  giving a local maximum for  $R_n(p_{T,n}, \beta^*)$ . After finding  $\beta^*$ , we can update  $p_{T,n}$  which is found by satisfying the minimum rate requirement where the rate is increasing in  $p_{T,n}$  (see Appendix C), i.e.,  $R_n(p_{T,n}, \beta^*) = R_{\min}$ .

### 4.2.1 Single window optimization

The next step is to find the optimal resource allocation in the case of one transmission window. The corresponding optimization problem reduces to

$$\begin{aligned} \min_{p_1} \quad & p_1 \\ \text{subject to} \quad & R_1 \geq R_{\min} \\ & 0 \leq p_1 \leq p_{\max}. \end{aligned} \quad (17)$$

The rate  $R_1$  can be expressed as

$$R_1(p_1) = Bk_1(1 - \eta_1(p_1)), \quad (18)$$

where

$$\begin{aligned} \eta_1(p_1) = & 4 \left(1 - \frac{1}{\sqrt{M_1}}\right) \mathcal{Q} \left( \sqrt{\frac{3}{M_1 - 1} G_t G_r \Gamma_1 p_1 P_{\text{shaping}}} \right) \\ & - 4 \left(1 - \frac{1}{\sqrt{M_1}}\right)^2 \mathcal{Q} \left( \sqrt{\frac{3}{M_1 - 1} G_t G_r \Gamma_1 p_1 P_{\text{shaping}}} \right)^2 \end{aligned} \quad (19)$$

Since the rate is increasing in  $p_1$  then, the solution  $p_1^*$  will be as following

- If  $R_1(p_{\max}) \geq R_{\min}$ , then,  $p_1^*$  is such that  $R_1(p_1^*) = R_{\min}$ .
- Otherwise  $p_1^* = 0$ .

Then, the modulation scheme is found through a basic search among the feasible space of  $k$ . The optimization process is summarized in Algorithm 1.

---

**Algorithm 1** Recursive Algorithm for Resource Allocation

```

1: input:  $p_{\max}, k_{\max}$ 
2:  $p_{\bar{n}} = p_{\max}$ 
3: Compute  $P_1^*, k_1^*$  as described in Section 4.2.1.
4:  $p_{\Gamma} = P_1^*$ 
5: if  $R_n(p(\beta_n^*, p_{\max})) \geq R_{\min}$  then
6:   compute  $p_{\Gamma_n}$  such that  $R(p(\beta_n^*, p_{\Gamma_n})) = R_{\min}$ 
7: else
8:    $p_{\Gamma_n} = 0$ 
9: end if
10: for  $n = 2 : L$  do
11:    $\alpha(\beta) = [\beta\alpha^* \ 1 - \beta]$ 
12:    $p(\beta, p_{\bar{n}}) = p_{\bar{n}}\alpha(\beta)$ 
13:    $\beta_n^* = \arg \max_{\beta \in [0,1]} R(p(\beta, p_{\bar{n}}))$ 
14:   if  $R_n(p(\beta_n^*, p_{\max})) \geq R_{\min}$  then
15:     compute  $p_{\Gamma_n}$  such that  $R(p(\beta_n^*, p_{\Gamma_n})) = R_{\min}$ 
16:   else
17:      $p_{\Gamma_n} = 0$ 
18:   end if
19:    $p_{\Gamma_n}^* = \min_{p_{\Gamma_n} \neq 0} p_{\Gamma_n}$ 
20:   if  $p_{\Gamma_n}^* \neq 0$  then
21:      $p_{\bar{n}} = p_{\Gamma_n}^*$ 
22:      $\alpha^* = \alpha(\beta_n^*)$ 
23:      $k_n^* = \arg \min_{1 \leq k \leq k_{\max}} p_{\Gamma_n}(k)$ 
24:   else
25:      $p_{\bar{n}} = p_{\max}$ 
26:      $\alpha^* = \frac{2}{n(n+1)}[n, \dots, 1]$ 
27:      $k_n^* = \arg \max R_n(\alpha^*, p_{\max})$ 
28:   end if
29: end for

```

---

#### 4.2.2 Recursive algorithm

The resource allocation algorithm developed in this study is recursive. The power distribution factors, the total allocated power and the number of allocated bits of each iteration are the input to the next. The modulation is found through a basic search over the discrete set of modulation orders.

The optimization process adopted in this work is summarized in Algorithm 1. As a first step, in line 3 the algorithm solves the single window case and computes the optimal solution of the problem in (17) as explained in Section 4.2.1. Then, the solution will be the input to solve the two windows case. Therefore, the algorithm uses the solution of one window case to recursively compute the optimized allocated resource for all channels, while guaranteeing that using extra channels will improve the solution and meet the operational constraints. After each iteration  $n$ , the power distribution factors over  $n$  windows, the total allocated power, and the modulation scheme will serve as an input for iteration  $n + 1$ . At iteration  $n$ , the algorithm finds the power distribution that maximizes the rate (line 13). Next, the total power  $p_{\Gamma_n}$  is computed in a way that  $R_{\min}$  is reached (line 15). If a solution is found, the algorithm computes  $k_n$  that minimizes the power (line 23). Otherwise, the input of the next iteration is  $p_{\max}$  as a total power, a distribution factor chosen as  $\alpha^* = \frac{2}{n(n+1)}[n, \dots, 1]$  and  $k_n$  that maximizes the rate (lines 25, 26 and 27).

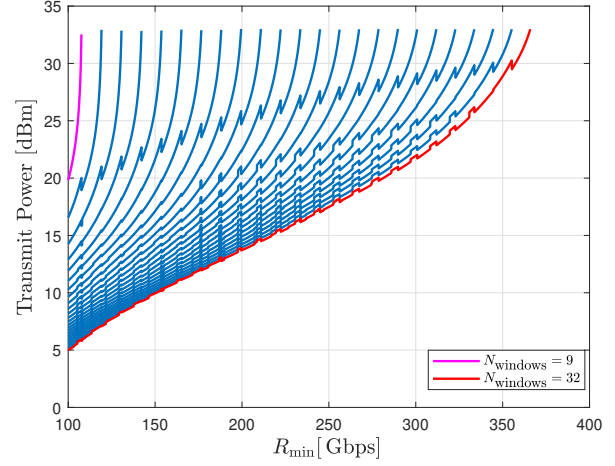


Figure 5: Transmit power versus  $R_{\min}$  for different numbers of allocated windows, from 1 window to 32 windows.

## 5 SIMULATION RESULTS

In this section, we study the benefits of using the proposed optimization method. Throughout different simulation examples, we investigate the impact of different system parameters on the transmit power. We use the following simulation parameters unless otherwise specified; we consider  $p_{\max} = 2W$ . The pathloss is computed as explained in section 2. As mentioned before, in this system, we consider high antenna gains,  $G_t = 30$  dB and  $G_r = 30$  dB, to ensure an aligned directed beam, prevent reflections and help beat the high link attenuation. The humidity level is set to 10% and the distance to 20 m, unless otherwise specified.

First, we compare the optimized power using different numbers of windows for different system requirements. As such, we plot the transmit power versus  $R_{\min}$  in Fig. 5. As it was mentioned in the system design part, using all the available windows helps reducing the transmit power and eventually, the possibility to convey higher rates. For this reason, the curve representing the use of all the 32 windows represents the optimized design. The discontinuity at each of the plotted curves is due to the recursive nature of the proposed allocation algorithm, i.e., where each iteration depends on the previous one. The sudden change in the input power, modulation and distribution factors causes discontinuities at some points. For example, the discontinuity of the curve of  $N_{\text{windows}} = 10$  happens at  $R_{\min}$  where the curve of  $N_{\text{windows}} = 9$  solution becomes infeasible. At this point, the parameters of the 9-windows allocation (total transmit power, power allocation factors, and modulation) can not be used as an input in the 10-windows allocation. The 10-windows system exhibits discontinuities at this point due to changing the initial point computation way. Another reason for the discontinuities is using the same number of bits of low bands after increasing the number of windows. Both behaviors occur at other parts of the curves with different transmission windows, causing the observed discontinuities. Additionally, for the considered range of  $R_{\min}$ , allocating less than 9 windows

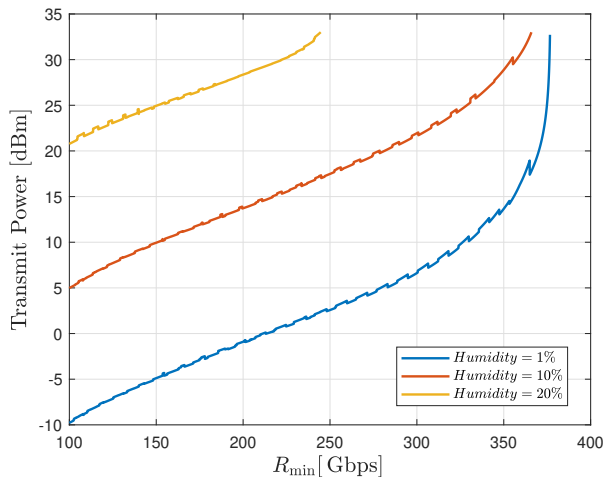


Figure 6: Transmit power versus  $R_{\min}$  for different humidity levels.

cannot achieve the system's requirement making the use of more windows imperative. Using 32 windows, the data rate can reach 360 Gbps, while its maximum value is 150 Gbps when the system transmits over 13 windows.

In the second simulation example, we investigate the effect of humidity on the transmit power. As such, we plot the optimized power versus  $R_{\min}$  when all the available windows are accessed and for different humidity levels in Fig.6. The figure shows that the system consumes an additional 15 dBm of power when humidity increases from 1% to 10% and almost the same difference in the consumed power when the humidity increases from 10% and 20%.

As the humidity increases, the system is forced to spend more power. For this reason, at a certain value of humidity, the system will not be able to operate reliably (depending on the maximum budget). Furthermore, the maximum  $R_{\min}$  that the system can convey differ with humidity. When the humidity is 20%, the system can convey almost 250 Gbps at most, while for 1% humidity level, the system can reach 370 Gbps. Since humidity is a critical parameter to take into consideration when deploying a THz communication link, it is important to set maximum allowable humidity levels for a solid operation of the system. **Therefore, environments suffering high humidity levels or rainy weather may not be eligible for outdoor THz communication systems. The wireless signal can be completely lost, causing the wireless connection to drop.**

In the next simulation example, we plot in Fig. 7, the power saving percentage with respect to the transmission range for different numbers of windows, with a minimum rate of 100 Gbps and 200 Gbps. First of all, we can observe that, for the considered **atmospheric** conditions and system requirements, the maximum distance that can be reached is almost 38 meters when  $R_{\min} = 200$  Gbps and 50 meters when  $R_{\min} = 100$  Gbps, if we use all the available bandwidth. This is expected because for higher  $R_{\min}$ , the system spends more power for the same distance. Second, when  $R_{\min} = 100$  Gbps, the gain in terms of transmission range earned from using 32 windows over 17 windows is almost 5

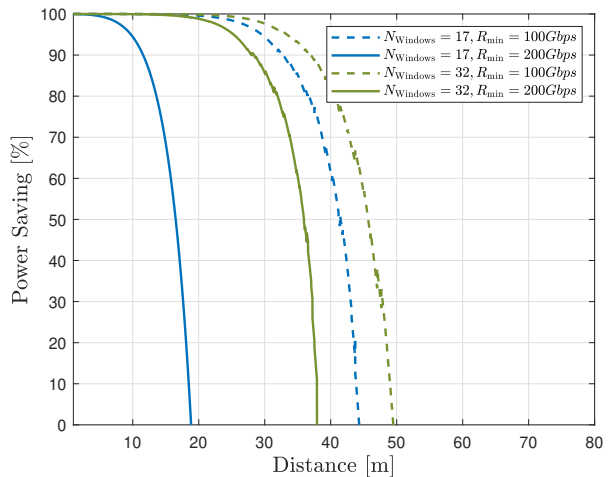


Figure 7: Power saving versus the distance for different numbers of windows and different  $R_{\min}$ .

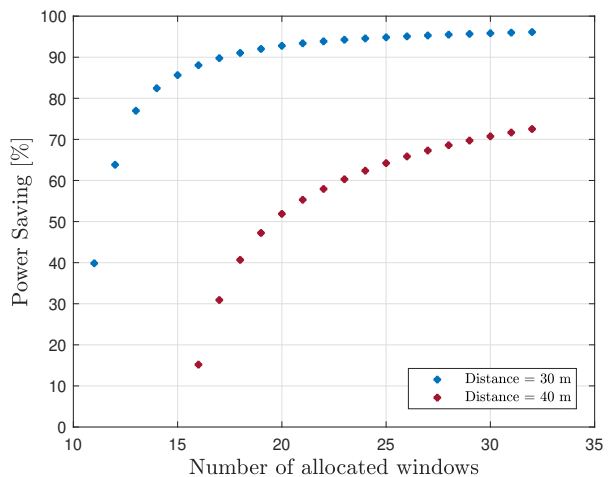


Figure 8: Power saving versus the number of allocated windows.

meters, while for  $R_{\min} = 200$  Gbps, it is around 20 meters. In fact, when  $R_{\min}$  increases, small numbers of windows become gradually incapable of supporting larger minimum required rates. Then, the benefit of using 32 windows over 17 windows becomes more explicit at higher  $R_{\min}$ . For this reason, the distance gain between 17 and 32 windows is more significant for larger  $R_{\min}$ .

In Fig.8, we plot the power saving versus the number of allocated windows for different distances when  $R_{\min} = 120$  Gbps. First of all, the figure shows that using less than 11 windows for the considered parameters cannot achieve the minimum required rate. As the number of windows increases, the system has a wider room to increase the transmit rate and therefore consume less power. Consequently, utilizing all the available windows boosts the system's capability and promotes power saving. Certainly, when the

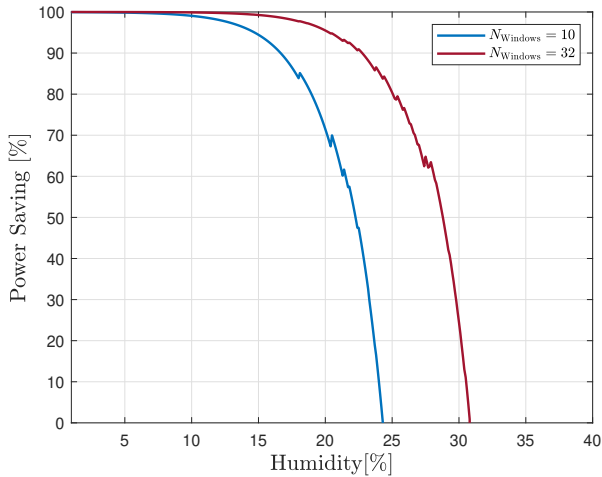


Figure 9: Power saving versus the humidity for different numbers of windows.

receiver is farther from the transmitter, pathloss increases and with it the need for more power. This phenomenon, as previously explained, is more intensified in the THz band due to the molecular attenuation. We observe in the figure, that when 20 windows are used, a 40% gain in power consumption is obtained for 10 meters difference in distance. Moreover, when the number of utilized windows increases, the difference in power saving between 30 meters and 40 meters of distance decreases. This can be explained by the fact that, when the available bandwidth becomes wider, the effect of the transmission distance becomes less significant. However, the covering range of a THz system is still one of the most crucial factors to account for because of the severe attenuation. For this reason, THz waves are known to better operate at short distances and long-range transmissions require high gain antennas and proper environments.

In this simulation example, we plot in Fig.9, the power saving versus the humidity for two numbers of transmission windows when  $R_{\min} = 80$  Gbps. The figure shows that the transmission is not possible after a certain humidity threshold. In fact, humidity is one of the most important factors that affect the THz wave, the latter being considerably absorbed by water molecules. Consequently, designing systems operating at THz frequencies must take into consideration the humidity levels of the transmission environment. The benefit reaped from accessing all the available bandwidth is substantial in terms of maximum allowable humidity level. As shown in the figure, allocating the entire available bandwidth (32 windows) improves the tolerance of the system to humidity and therefore, creates a tremendous advantage for the system to be deployed in more severe environments.

For the last simulation example, we plot in Fig.10, the modulation scheme versus the number of the allocated window when  $R_{\min} = 100$  Gbps. We consider the best case, which is the use of all 32 windows. The modulation orders considered in the design are 4QAM, 16QAM, 64QAM and 256QAM. The figure shows that the modulation order decreases when the pathloss over a window increases. This

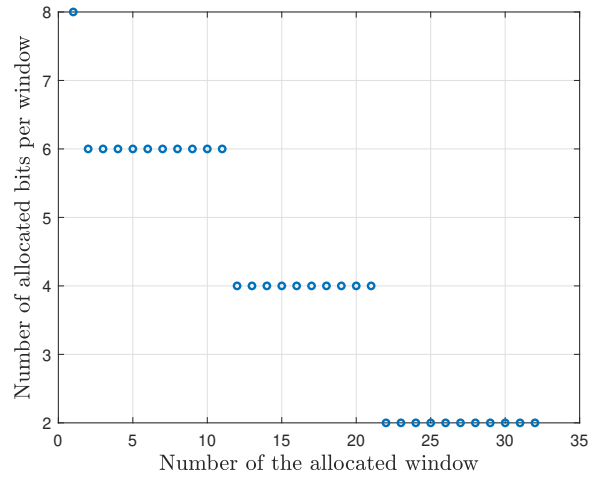


Figure 10: Modulation scheme per transmission window.

is justified by the fact that higher modulation orders need higher SNR to keep the minimum distance between symbols in a QAM constellation and avoid detection errors.

## 6 CONCLUSION

Since the usual frequency bands are now critically saturated because of the expansion of wireless applications, THz band has gained attention since it is not yet utilized and it offers wide-band communications and very high data rates. In this paper, we described the pathloss in the THz band which is characterized by the additional molecular absorption. We summarized the approach to compute the pathloss model for specific **atmospheric** conditions represented as temperature, pressure and mainly humidity. Then, we proposed a system with one user, trying to access the THz channel, as defined by the THz standard, that strategically allocates power, bandwidth and modulation to convey a minimum required rate while minimizing its transmit power. It was shown that allocating all the available windows helps optimizing power consumption since, the capacity of the channel increases creating a larger room to increase the data rate, and hence reduce the transmit power. Furthermore, we attempted to inspect the effect of humidity, as a key parameter in THz communication, on the system's behavior. Singularly, increasing the amount of water vapor in the air considerably reduces the performance of the system and can jeopardize its proper operation. This is evoked by the significant increase of pathloss and the more pronounced absorption peaks.

## REFERENCES

- [1] A. A. Ateya, A. Muthanna, M. Makolkina, and A. Koucheryavy, "Study of 5G services standardization: specifications and requirements," in *IEEE 10th Int. Congress Ultra Modern Telecommun. Control Sys. Workshops (ICUMT)*, 2018, pp. 1–6.
- [2] S. Dang, O. Amin, B. Shihada, and M.-S. Alouini, "What should 6G be?" *Nature Electron.*, vol. 3, no. 1, pp. 20–29, 2020.

- [3] A. Hirata, T. Kosugi, H. Takahashi, J. Takeuchi, K. Murata, N. Kukutsu, Y. Kado, S. Okabe, T. Ikeda, F. Suginosita *et al.*, "5.8-km 10-Gbps data transmission over a 120-GHz-band wireless link," in *IEEE Int. Conf. Wireless Inf. Technol. Syst.*, Honolulu, HI, USA, Sept. 2010, pp. 1–4.
- [4] T. Kleine-Ostmann and T. Nagatsuma, "A review on Terahertz communications research," *J. Infrared, Millimeter, THz. Waves*, vol. 32, no. 2, pp. 143–171, 2011.
- [5] H.-J. Song and T. Nagatsuma, "Present and future of Terahertz communications," *IEEE Trans. THz Sci. Technol.*, vol. 1, no. 1, pp. 256–263, 2011.
- [6] M. M. Ahamed and S. Faruque, "5G Backhaul: Requirements, Challenges, and Emerging Technologies," *Broadband Communications: Recent Advances and Lessons from Practice*, p. 43, 2018.
- [7] A. Moldovan, M. A. Ruder, I. F. Akyildiz, and W. H. Gerstacker, "LoS and NLoS channel modeling for Terahertz wireless communication with scattered rays," in *IEEE Globecom Workshops*, 2014, pp. 388–392.
- [8] C. Jansen, S. Priebe, C. Moller, M. Jacob, H. Dierke, M. Koch, and T. Kurner, "Diffuse scattering from rough surfaces in THz communication channels," *IEEE Trans. THz Sci. Technol.*, vol. 1, no. 2, pp. 462–472, 2011.
- [9] T. Kurner, R. Piesiewicz, M. Koch, and J. Schoebel, "Propagation models, measurements and simulations for wireless communication systems beyond 100 GHz," in *IEEE Int. Conf. Electromagn. Advanced Appl.*, Torino, Italy, Sept. 2007, pp. 108–111.
- [10] R. Piesiewicz, C. Jansen, D. Mittleman, T. Kleine-Ostmann, M. Koch, and T. Kurner, "Scattering analysis for the modeling of THz communication systems," *IEEE Trans. Antennas Propag.*, vol. 55, no. 11, pp. 3002–3009, 2007.
- [11] C. Han, A. O. Bicen, and I. F. Akyildiz, "Multi-ray channel modeling and wideband characterization for wireless communications in the Terahertz band," *IEEE Trans. Wireless Commun.*, vol. 14, no. 5, pp. 2402–2412, 2015.
- [12] K. Tsujimura, K. Umabayashi, J. Kokkonen, J. Lehtomäki, and Y. Suzuki, "A Causal Channel Model for the Terahertz Band," *IEEE Trans. THz Sci. Technol.*, vol. 8, no. 1, pp. 52–62, 2018.
- [13] Y. Chen and C. Han, "Channel modeling and analysis for wireless networks-on-chip communications in the millimeter wave and Terahertz bands," in *IEEE INFOCOM Conf. Comput. Commun. Workshops*, Honolulu, HI, USA, Apr. 2018.
- [14] C. Han and I. F. Akyildiz, "Distance-aware bandwidth-adaptive resource allocation for wireless systems in the Terahertz band," *IEEE Trans. THz Sci. Technol.*, vol. 6, no. 4, pp. 541–553, 2016.
- [15] C. Han, A. O. Bicen, and I. F. Akyildiz, "Multi-wideband waveform design for distance-adaptive wireless communications in the Terahertz band," *IEEE Trans. Signal Process.*, vol. 64, no. 4, pp. 910–922, 2016.
- [16] D. Li, D. Qiao, and L. Zhang, "Achievable Rate of Indoor THz Communication Systems with Finite-Bit ADCs," in *IEEE 10th Int. Conf. Wireless Commun. Signal Process. (WCSP)*, Hangzhou, China, Oct. 2018, pp. 1–6.
- [17] X.-W. Yao, C.-C. Wang, W.-L. Wang, and J. M. Jornet, "On the achievable throughput of energy-harvesting nanonetworks in the Terahertz band," *IEEE Sensors J.*, vol. 18, no. 2, pp. 902–912, 2018.
- [18] Y. Pan, K. Wang, C. Pan, H. Zhu, and J. Wang, "Sum rate maximization for intelligent reflecting surface assisted terahertz communications," *arXiv preprint arXiv:2008.12246*, 2020.
- [19] X. Ma, Z. Chen, W. Chen, Z. Li, Y. Chi, C. Han, and S. Li, "Joint channel estimation and data rate maximization for intelligent reflecting surface assisted terahertz MIMO communication systems," *IEEE Access*, vol. 8, pp. 99 565–99 581, 2020.
- [20] H. Zhang, H. Zhang, W. Liu, K. Long, J. Dong, and V. C. Leung, "Energy efficient user clustering, hybrid precoding and power optimization in terahertz MIMO-NOMA systems," *IEEE Journal on Selected Areas in Communications*, vol. 38, no. 9, pp. 2074–2085, 2020.
- [21] M. Yu, A. Tang, X. Wang, and C. Han, "Joint scheduling and power allocation for 6G terahertz mesh networks," in *IEEE International Conference on Computing, Networking and Communications (ICNC)*, 2020, pp. 631–635.
- [22] A. Moldovan, P. Karunakaran, I. F. Akyildiz, and W. H. Gerstacker, "Coverage and achievable rate analysis for indoor terahertz wireless networks," in *IEEE Int. Conf. Commun. (ICC)*, Paris, France, May. 2017, pp. 1–7.
- [23] C. A. Balanis, *Antenna theory: analysis and design*, fourth;4th; ed. Hoboken, New Jersey: Wiley, 2016;2015;.
- [24] T. Schneider, A. Wiatrek, S. Preußler, M. Grigat, and R.-P. Braun, "Link budget analysis for Terahertz fixed wireless links," *IEEE Trans. THz Sci. Technol.*, vol. 2, no. 2, pp. 250–256, 2012.
- [25] S. Lee, S. Amakawa, T. Yoshida, Y. Morishita, Y. Kashino, S. Hara, and M. Fujishima, "300-ghz cmos-based wireless link using 40-db cassegrain antenna for ieee standard 802.15. 3d," in *2020 IEEE International Symposium on Radio-Frequency Integration Technology (RFIT)*. IEEE, 2020, pp. 136–138.
- [26] A. Martínez, I. Maestrojua, D. Valcazar, and J. Teniente, "High gain antenna for sub-millimeter wave communications," in *2016 46th European Microwave Conference (EuMC)*. IEEE, 2016, pp. 37–40.
- [27] I. E. Gordon, L. S. Rothman, C. Hill, R. V. Kochanov, Y. Tan, P. F. Bernath, M. Birk, V. Boudon, A. Campargue, K. Chance *et al.*, "The HITRAN2016 molecular spectroscopic database," *J. Quantitative Spectrosc. Radiative Transfer*, vol. 203, pp. 3–69, 2017.
- [28] J. M. Jornet and I. F. Akyildiz, "Channel modeling and capacity analysis for electromagnetic wireless nanonetworks in the Terahertz band," *IEEE Trans. Wireless Commun.*, vol. 10, no. 10, pp. 3211–3221, 2011.
- [29] L. S. Rothman, I. E. Gordon, A. Barbe, D. C. Benner, P. F. Bernath, M. Birk, V. Boudon, L. R. Brown, A. Campargue, J.-P. Champion *et al.*, "The HITRAN 2008 molecular spectroscopic database," *J. Quantitative Spectrosc. Radiative Transfer*, vol. 110, no. 9–10, pp. 533–572, 2009.
- [30] "THz Communications – An Overview and Options for IEEE 802 Standardization, Project: IEEE P802.15 Working Group for Wireless Personal Area Networks (WPANs)," Available at <https://mentor.ieee.org/802.15/dcn/18/15-18-0516-01-0thz-tutorial-thz-communications-an-overview-and-options-for-ieee-802-standardization.pdf>.
- [31] "IEEE standard for high data rate wireless multi-media networks—amendment 2: 100 Gb/s wireless switched point-to-point physical layer," *Amendment to IEEE Std 802.15.3-2016 as amended by IEEE Std 802.15.3e-2017*, pp. 1–55, Oct. 2017.
- [32] H. Elayan, O. Amin, B. Shihada, R. M. Shubair, and M.-S. Alouini, "Terahertz band: The last piece of RF spectrum puzzle for communication systems," *IEEE Open J. Commun. Soc.*, vol. 1, pp. 1–32, 2019.
- [33] V. Petrov, T. Kurner, and I. Hosako, "IEEE 802.15. 3d: First Standardization Efforts for Sub-Terahertz Band Communications toward 6G," *IEEE Commun. Mag.*, vol. 58, no. 11, pp. 28–33, 2020.
- [34] K. M. S. Huq, S. A. Busari, J. Rodriguez, V. Frascolla, W. Bazzi, and D. C. Sicker, "Terahertz-enabled wireless system for beyond-5g ultra-fast networks: A brief survey," *IEEE Netw.*, vol. 33, no. 4, pp. 89–95, 2019.
- [35] K. Tsujimura, K. Umabayashi, J. Kokkonen, J. Lehtomäki, and Y. Suzuki, "A causal channel model for the Terahertz band," *IEEE Trans. THz Sci. Technol.*, vol. 8, no. 1, pp. 52–62, 2017.
- [36] C. Zhang, C. Han, and I. F. Akyildiz, "Three dimensional end-to-end modeling and directivity analysis for graphene-based antennas in the Terahertz band," in *IEEE Global Commun. Conf. (GLOBECOM)*, San Diego, CA, USA, Dec. 2015, pp. 1–6.
- [37] A. V. Oppenheim and R. W. Schaffer, *Digital signal processing*. Prentice Hall, 1975.
- [38] J. G. Proakis and M. Salehi, *Digital communications*. McGraw-hill New York, 2001, vol. 4.



**Wafa Hedhly** received the Telecommunication Engineering degree from the Higher School of Communications of Tunis (Sup'Com), Ariana, Tunisia, in 2017 and the M.Sc. degree in Electrical Engineering from the King Abdullah University of Science and Technology (KAUST), Thuwal, Saudi Arabia, in 2019, where she is currently pursuing the Ph.D. degree. Her research interests include channel modeling, Terahertz communication and Hyperloop communication systems.

PLACE  
PHOTO  
HERE

**Osama Amin** (S'07, M'11, SM'15) received his B.Sc. degree in electrical and electronic engineering from Aswan University, Egypt, in 2000, his M.Sc. degree in electrical and electronic engineering from Assiut University, Egypt, in 2004, and his Ph.D. degree in electrical and computer engineering, University of Waterloo, Canada, in 2010. In June 2012, he joined Assiut University as an assistant professor in the Electrical and Electronics Engineering Department. Currently, he is a research scientist in the CEMSE Division at KAUST, Thuwal, Makkah Province, Saudi Arabia. His general research interests lie in communication systems and signal processing for communications with special emphasis on wireless applications.

of Electrical Engineering in 2009. His current research interests include modeling, design, and performance analysis of wireless communication systems.

PLACE  
PHOTO  
HERE

**Mohamed-Slim Alouini** (S'94-M'98-SM'03-F'09) was born in Tunis, Tunisia. He received the Ph.D. degree in Electrical Engineering from the California Institute of Technology (Caltech), Pasadena, CA, USA, in 1998. He served as a faculty member in the University of Minnesota, Minneapolis, MN, USA, then in the Texas A&M University at Qatar, Education City, Doha, Qatar before joining King Abdullah University of Science and Technology (KAUST), Thuwal, Makkah Province, Saudi Arabia as a Professor

of Electrical Engineering in 2009. His current research interests include modeling, design, and performance analysis of wireless communication systems.

PLACE  
PHOTO  
HERE

**Basem Shihada** is an associate and founding professor in the Computer, Electrical and Mathematical Sciences and Engineering (CEMSE) Division at King Abdullah University of Science and Technology (KAUST). He obtained his PhD in Computer Science from University of Waterloo. In 2009, he was appointed as visiting faculty in the Department of Computer Science, Stanford University. In 2012, he was elevated to the rank of Senior Member of IEEE. His current research covers a range of topics in energy and resource

allocation in wired and wireless networks, software defined networking, cloud/fog computing, internet of things, data networks, and underwater networks.